Advances in Differential Equations and Control Processes 2025, 32(2), 2818.
https://doi.org/10.59400/adecp2818

Article

Weak fault diagnosis method for rotorcraft bearings based on whale optimization algorithm—Optimized simplistic geometry mode decomposition and maximum correlated kurtosis deconvolution

Liang Gao, Changhong Li*

School of electronic information engineering, Xi'an Technological University, Shaanxi 710021, China
*** Corresponding author:** Changhong Li, lichanghong01@xatu.edu.cn

CITATION

Liang G, Li C. Weak fault diagnosis method for rotorcraft bearings based on whale optimization algorithm—Optimized simplistic geometry mode decomposition and maximum correlated kurtosis deconvolution. Advances in Differential Equations and Control Processes. 2025; 32(2): 2818. https://doi.org/10.59400/adecp2818

ARTICLE INFO

Received: 20 February 2025
Accepted: 27 April 2025
Available online: 12 May 2025

Abstract: Early fault signals of the rolling bearing in the rotor are weak and present the characteristics of non-periodic and non-stationary; it is more difficult to carry out fault diagnosis on it. In this regard, this paper proposes a weak rolling bearing fault diagnosis algorithm based on whale optimization algorithm, simplistic geometry mode decomposition, and maximum correlated kurtosis deconvolution (WOA-SGMD-MCKD). Firstly, the vibration signal of the rotor platform is obtained, and the Symmetric Geometric Mode Decomposition (SGMD) is used to reconstruct the vibration signal. To obtain the best decomposition effect of the SGMD and overcome modal aliasing, the Whale Optimization Algorithm (WOA) is used to optimize the embedding dimension. Secondly, for the reconstructed vibration signal, the Maximum Correlated Kurtosis Deconvolution (MCKD) is used to extract its impulse component, and the WOA is used to optimize the filter length and deconvolution period of the MCKD so that the frequency envelope spectrum of the vibration signal can be obtained, which can provide the basis for the fault diagnosis of rolling bearings. Finally, the effectiveness and feasibility of the algorithm proposed are verified by a non-periodic and non-stationary simulation platform and rotor maneuvering platform in this paper.

Keywords: rolling bearing; SGMD; MCKD; WOA

1. Introduction

Rotor blades are an important part of an unmanned aerial vehicle (UAV), providing power for the UAV to fly. As the key part of rotor components, rolling bearings work in an environment with high rotational speeds and complex loads and are susceptible to the influence of dust and acid mist in the environment, resulting in wear, fatigue spalling, corrosion, abrasion, fracture, and other problems of rolling bearings [1]. However, extracting the early fault characteristics from rolling bearings can be extremely challenging, primarily due to the subtle and weak impacts generated by these initial faults, which are affected by the strong noise of the UAV, and its fault signal is characterized by non-linearity and non-smoothness. Therefore, identifying and enhancing the weak fault signals of rolling bearings amidst strong noise environments is crucial for enabling early fault diagnosis of rotary wing systems. The key lies in devising effective methods to extract and amplify these fault characteristics.

The fault diagnosis method of rolling bearings is mainly for the original vibration signal to make signal reconstruction, fault feature extraction, fault pattern recognition and other processes [2]. Currently, the prevalent approaches for rolling bearing fault diagnosis encompass a diverse range of methodologies, including time domain analysis, frequency domain analysis, time-frequency domain analysis, as well as the

utilization of neural networks and other advanced techniques [3]. The time domain analysis method is mainly used to extract the statistical features such as mean, variance, and crag of the fault time series signal for the characterization of the fault signal. The frequency domain method is mainly based on Fast Fourier Transform (FFT) analysis to extract the spectrum of the fault signal. The time-frequency domain analysis methods are mainly wavelet decomposition, sparse decomposition, and empirical modal decomposition method [4]. Literature [5] proposed a rolling bearing fault diagnosis algorithm based on FFT and multi-feature parallel fusion encoder, which is suitable for periodic fault signals. Literature [6] presents a rolling bearing fault diagnosis algorithm that innovatively combines wavelet transform with convolutional neural network, offering a unique approach to the task, the accuracy of the fault diagnosis algorithm is effectively improved, but the fixed basis function of wavelet decomposition still exists the problem of poor self-adaptation. In Literature [7], a novel algorithm for rolling bearing fault diagnosis is introduced, which is fundamentally based on the concept of clustered weighted envelope spectrum. Literature [8] proposed a rolling bearing fault diagnosis algorithm based on restricted sparse network. However, the methods proposed in the literature [5–8] have the problem of inaccurate fault feature extraction in the process of solving the non-periodic and non-stationary rolling bearing fault signals. Therefore, for the non-periodic and non-stationary characteristics in bearing fault signals, literature [9] proposed an algorithm for extracting fault features in rolling bearings based on empirical modal decomposition (EMD). It acknowledges that this method faces challenges such as modal aliasing and the endpoint effect, which can compromise its accuracy and reliability. Literature [10] proposed a rolling bearing feature extraction algorithm for variational modal decomposition (VMD), but the VMD decomposition has the problem that the number of decompositions is difficult to determine. In recent years, the fault diagnosis algorithm based on Symplicit Geometric Modal Decomposition (SGMD) has been proposed for fault diagnosis of rotating machinery, which has the advantages of clear physical meaning, noise robustness, and good adaptability because it effectively preserves the intrinsic characteristics of time series data [11].

However, the complex operating environment, severe noise interference, multiple vibrations, and motor rotations coupled with each other in a rotorcraft make early failure extraction of rotorcraft rolling bearings more difficult. In this regard, literature [12] proposed an enhanced envelope analysis and blind deconvolution technique for weak fault diagnosis of rolling bearings. Literature [13] introduced an innovative approach for fault diagnosis of rolling bearings, which integrates an adaptive time-varying filtering technique with an order tracking algorithm to enhance diagnostic accuracy and effectiveness. However, the algorithms proposed in the literature [12,13] do not adequately consider the time-varying, strongly noisy operating environments in which rotor blades operate. At present, as one of the current mainstream algorithms for fault signal enhancement, the maximum correlated kurtosis deconvolution (MCKD) algorithm has the advantages of strong noise immunity, good self-adaptation, and effective elimination of the influence of the signal transmission path, and it is widely used in the enhancement of weak fault signals [14–16].

In summary, for the non-periodic, non-smooth, and strong noise effects of the early fault signals of rotor rolling bearings, the paper adopts SGMD to extract the fault characteristics of all of its components and MCKD to enhance the impact pulse of the fault signals and then completes the early fault diagnosis of rotor rolling bearings. However, the number of decompositions of SGMD and the filter length parameter and deconvolution period parameter of MCKD have an important impact on the effectiveness of the rotor bearing fault diagnosis algorithm. In order to select the appropriate algorithm, in this paper, the whale optimization algorithm (WOA) is selected as the optimization tool to fine-tune the parameters of SGMD and MCKD models, aiming to achieve optimal performance. Finally, the algorithm proposed in the paper is validated on a rotor platform.

2. Basic methodological principle

2.1. Symplectic geometry mode decomposition (SGMD)

SGMD (symmetric geometric mode decomposition) represents a pioneering approach to signal decomposition that commences by meticulously reconstructing the phase space of the original signal. And determines the embedding dimensions and the trajectory matrix using the power spectral density (PSD) method; then constructs the Hamiltonian matrix and solves its eigenvalues using the symplectic geometry similarity transform; finally, diagonal averaging and adaptive reconstruction techniques are employed to extract the symplectic geometry component (SGC). The method is characterized by invariant intrinsic characteristics of the time series, suppression of modal confusion, removal of noise in the process of efficiently reconstructing a single component, and does not require the definition of any subjective parameters. Specific realization process:

(1) Phase space reconstruction. Assuming that the original signal series is $\boldsymbol{x} = (x_1, x_2, \ldots, x_n)$ (n is the sample number), phase space reconstruction via the Takens Embedding Theorem involves constructing a higher-dimensional space from a single time series by embedding delayed versions of the series; the trajectory matrix $\boldsymbol{X}$ can be obtained.

$$X = \begin{bmatrix} x_1 & x_{1+\tau} & \cdots & x_{1+(d-1)\tau} \\ x_2 & x_{2+\tau} & \cdots & x_{2+(d-1)\tau} \\ \vdots & \vdots & \ddots & \vdots \\ x_m & x_{m+\tau} & \cdots & x_{m+(d-1)\tau} \end{bmatrix} \tag{1}$$

where τ is delay time, d is embedding dimension, and $m = n - (d-1)\tau$.

For Equation (1), the result of the trajectory matrix $\boldsymbol{X}$ is determined by the values of the parameters τ and d. The delay time τ can be determined by the C-C algorithm, and the embedding dimension d can be determined by the PSD method. Calculate the PSD value of the original signal $\boldsymbol{x}$ and obtain the frequency f_{max} corresponding to the highest peak value of the PSD. Assuming that the sampling frequency is f_s and the threshold is ε (generally taking the value of 0.001), after the frequency normalization process, if $f_{max}/f_s > \varepsilon$, the embedding dimension $d = 1.2f_{max}/f_s$; conversely, the embedding dimension $d = n/3$.

(2) Hamiltonian matrix construction. Autocorrelation analysis is performed on the trajectory matrix $\boldsymbol{X}$ to obtain the corresponding covariance symmetry matrix $\boldsymbol{P}$:

$$\boldsymbol{P} = \boldsymbol{X}^{\mathrm{T}}\boldsymbol{X} \tag{2}$$

The Hamiltonian matrix $\boldsymbol{M}$ can be constructed based on the covariance symmetric matrix $\boldsymbol{P}$:

$$M = \begin{bmatrix} A^T & 0 \\ 0 & -A \end{bmatrix} \tag{3}$$

(3) Symplectic geometry similarity transform. Let $\boldsymbol{N} = \boldsymbol{M}^2$ and the matrix $\boldsymbol{N}$ is also a Hamiltonian matrix; an orthonormal matrix $\boldsymbol{Q}$ can be constructed to make

$$Q^T N Q = \begin{bmatrix} B^T & R \\ 0 & B \end{bmatrix} \tag{4}$$

where $\boldsymbol{B}$ is the upper triangular matrix and $\boldsymbol{R}$ is the transformed submatrix.

(4) Eigenvalue solving. $\boldsymbol{B}$ is an upper triangular matrix, i.e., $b_{ij} = 0$ ($i > j + 1$). The eigenvalues of matrix $\boldsymbol{B}$ are obtained from Schmidt orthogonalization as $\lambda_1, \lambda_2, \ldots, \lambda_d$, and the eigenvalues of matrix $\boldsymbol{A}$ are obtained from Hamiltonian matrix properties:

$$\sigma_i = \sqrt{\lambda_i}\ (i = 1, 2, \ldots\ldots, d) \tag{5}$$

The corresponding ground eigenvectors $\boldsymbol{Q}_i$ can be obtained from the eigenvalues of the matrix $\boldsymbol{A}$.

(5) Reconstruct the trajectory matrix $\boldsymbol{Z}$. Let $\boldsymbol{C} = \boldsymbol{Q}^T\boldsymbol{X}$, $\boldsymbol{Z} = \boldsymbol{QC}$; the reconstructed trajectory matrix $\boldsymbol{Z}$ can be obtained. The conversion factor matrix $\boldsymbol{C}$ is given by

$$C_i = Q_i^T X \tag{6}$$

The single-group trajectory matrix $\boldsymbol{Z}_i$ can be obtained after transforming the coefficient matrix $\boldsymbol{C}_i$:

$$Z_i = Q_i C_i \tag{7}$$

The reconstructed trajectory matrix $\boldsymbol{Z}$ consists of a single trajectory matrix $\boldsymbol{Z}_i$, and then there:

$$Z = Z_1 + Z_2 + \cdots + Z_d \tag{8}$$

(6) Diagonal averaging. Since the single-group trajectory matrix $\boldsymbol{Z}_i$ is an $m \times d$ matrix, the trajectory matrix $\boldsymbol{Z}_i$ needs to be reconverted into a signal with a sample size of n. Defined as z_{ij} ($1 \le i \le d$, $1 \le j \le m$) is the element of matrix $\boldsymbol{Z}_i$, let

$$z_{ij}^* = \begin{cases} z_{ij}, m < d \\ z_{ji}, m \ge d \end{cases} \tag{9}$$

The diagonally averaged transfer matrix is used to transform $\boldsymbol{Z}_i$ into a signal $\boldsymbol{Y}_i = (y_1, y_2, \ldots, y_k, \ldots, y_n)$ with a sample size of n:

$$y_k = \begin{cases} \frac{1}{k}\sum_{p=1}^{k} z^*_{p,k-p+1}, 1 \le k < d^* \\ \frac{1}{d^*}\sum_{p=1}^{d^*} z^*_{p,k-p+1}, d^* \le k \le m^* \\ \frac{1}{n-k+1}\sum_{p=k-m^*+1}^{n-m^*+1} z^*_{p,k-p+1}, m^* < k \le n \end{cases} \tag{10}$$

where $d^* = \min(m, d)$; $m^* = \max(m, d)$; $n = m + (d-1)\tau$.

By diagonal averaging, the d-group signals $\mathbf{Y}_i = (y_1, y_2, \ldots, y_k, \ldots, y_n)$ can be finally obtained.

(7) Signal extraction and reconstruction. The d-group signals are not completely independent of each other and still exhibit similarity. The signal is analyzed using the similarity criterion to calculate the similarity between a signal and the rest of the signals, and a linear superposition is applied to the signals that are more similar to it to obtain the l-th symplectic geometric component S_{GCl}, which is removed from the original signal, and the residual signal is noted as G_{h+1} (h is the number of iterations), and then there is:

$$G_{h+1} = x - \sum_{l=1}^{h} S_{GCl} \tag{11}$$

During each iteration, the G_{CSl} is removed from the original signal series $\boldsymbol{x}$ once, and the NMAE between the residual signal and the original signal decreases with the number of iterations; thus, the NMAE can be used as a sign of the similarity between the time series signals Y_i. To prevent the over-decomposition problem caused by too many iterations, NMAE is used as a new decomposition constraint, and different thresholds m are set according to the decomposition objects.

$$N_{MAEh} = \frac{1}{t}\sum_{t=1}^{n}\left|\frac{G_{h+1}(t)}{x(t)}\right| \tag{12}$$

If the NMAE is greater than the given threshold m, the residual signal G_{h+1} is first reconstructed to obtain the new trajectory matrix $\boldsymbol{X}_{m\times d}$; then the G_{CSl} is calculated again according to the above process, and it is eliminated from the residual signal G_{h+1}; finally, the NMAE is calculated and compared with the given threshold m until the NMAE is less than the given threshold m, the iterative process is ended, and the final result $x(t)$ is output.

$$x(t) = \sum_{h=1}^{N} S_{GCh}(t) + G_{N+1}(t) \tag{13}$$

where, N is the number of the *SGC*.

The flowchart is shown in **Figure 1**.

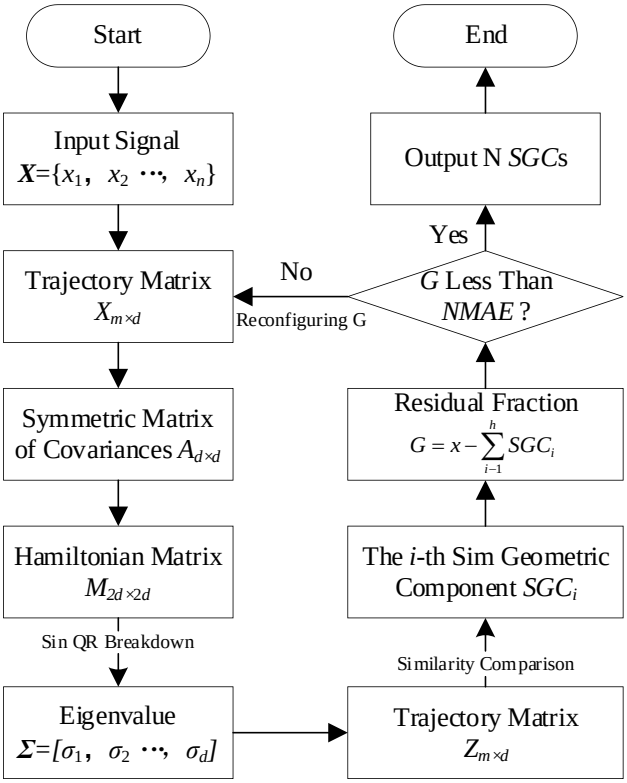

Figure 1. Flowchart of the SGMD method.

For complex and weak bearing signals, the SGMD method decomposes signals into multiple mode components. However, the decomposition is not good due to the strong noise effect, and in order to reduce the adverse effect of noise, the maximum correlated kurtosis deconvolution (MCKD) method can be used to complete feature extraction.

2.2. Maximum correlated kurtosis deconvolution (MCKD)

MCKD fully considers the periodicity of the shock component in the vibration signal and takes the correlation kurtosis as the optimization object, which can enhance the periodic shock component of the fault signal on the basis of effective noise reduction. The MCKD algorithm essentially maximizes the correlation kurtosis of the original periodic shock sequence by finding a series of FIR filters (f_l). The correlation cliff of the periodic shock signal y_i (i = 1, 2, …, N) can be defined as

$$CK_M(T) = \frac{\sum_{i=1}^{N}(\prod_{m=0}^{M} y_{i-mT})^2}{(\sum_{i=1}^{N} y_i^2)^{M+1}} \tag{14}$$

where T is the sample period of fault signals and M is the number of signal translation cycles.

With the correlation kurtosis as the optimization objective, an objective function can be established:

$$\max_f CK_M(T) = \max_f \frac{\sum_{i=1}^{N}(\prod_{m=0}^{M} y_{i-mT})^2}{(\sum_{i=1}^{N} y_i^2)^{M+1}} \tag{15}$$

Elements of the deconvolution signal $\boldsymbol{y}$ can be solved:

$$y_i = \sum_{k=1}^{L} f_k x_{i-k+1} \tag{16}$$

where, f_k is the filters; L is the step size of the filter.

The filter matrix can be expressed as

$$f = (f_1, f_2, \ldots, f_L)^T \tag{17}$$

An optimal filter can be identified to maximize the value of the correlation kurtosis $CK_M(T)$, then using the principle that the derivative is zero when a continuous function takes an extreme value, there is

$$\frac{d(CK_M(T))}{d(f_k)} = 0 \tag{18}$$

By calculating and organizing Equation (18), the expression for the filter matrix can be obtained:

$$f = \frac{||y^2||}{2||\beta||^2}(X_0 X_0^T)^{-1} \sum_{m=0}^{M} (X_{mT}\alpha_m) \tag{19}$$

where,

$$\beta = \begin{bmatrix} y_1 y_{1-T} y_{1-2T} \cdots y_{1-MT} \\ y_2 y_{2-T} y_{2-2T} \cdots y_{2-MT} \\ \vdots \\ y_N y_{N-T} y_{N-2T} \cdots y_{N-MT} \end{bmatrix};$$

$$X_0 = \begin{bmatrix} x_1 & x_2 & \cdots & x_N \\ 0 & x_1 & \cdots & x_{N-1} \\ \vdots & \vdots & \ddots & \vdots \\ 0 & 0 & \cdots & x_{N-L+1} \end{bmatrix}_{L\times N};$$

$$X_{mT} = \begin{bmatrix} x_{1-mT} & x_{2-mT} & \cdots & x_{N-mT} \\ 0 & x_{1-mT} & \cdots & x_{N-mT-1} \\ \vdots & \vdots & \ddots & \vdots \\ 0 & 0 & \cdots & x_{N-L-mT+1} \end{bmatrix}_{L\times N};$$

$$\alpha_m = \begin{bmatrix} y_{1-mT}^{-1}(y_1^2 y_{1-T}^2 y_{1-2T}^2 \cdots y_{1-MT}^2) \\ y_{2-mT}^{-1}(y_2^2 y_{2-T}^2 y_{2-2T}^2 \cdots y_{2-MT}^2) \\ \vdots \\ y_{N-mT}^{-1}(y_N^2 y_{N-T}^2 y_{N-2T}^2 \cdots y_{N-MT}^2) \end{bmatrix}_{N\times 1}.$$

Based on the preceding analysis, the specific implementation flowchart of MCKD method is shown in **Figure 2**.

In practical applications, the filter length L and sample period T of the MCKD method need to be manually set in advance, and unreasonable parameter settings can affect the results of signal processing. In order to achieve adaptive signal processing, intelligent algorithms can be used for parameter adaptive optimization to obtain a set of optimal parameter values and improve the accuracy and robustness of the algorithm.

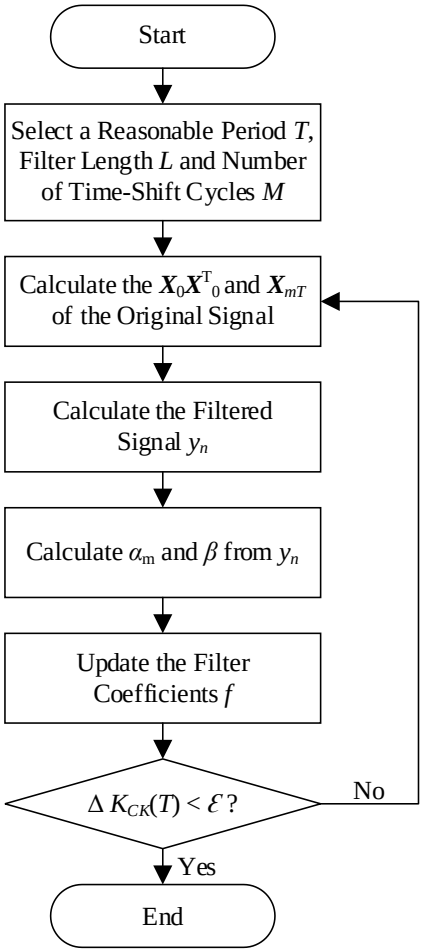

Figure 2. Flowchart of the MCKD method.

2.3. Whale optimization algorithm (WOA)

The whale optimization algorithm (WOA), a meta-heuristic optimization technique, is inspired by the hunting behavior of whales. In this algorithm, each whale's position signifies a potential solution. During the hunt, whales exhibit two primary behaviors: firstly, they converge towards each other to surround the prey, with all whales moving towards their peers; secondly, they engage in a bubble-net feeding method, where they swim in circular patterns and emit bubbles to herd their target. In each iteration, whales randomly select between these two strategies to optimize their hunt, using random or optimal search agents to simulate hunting behavior, effectively avoiding premature convergence and improving the algorithm's global search ability. At the same time, it has the advantages of not requiring gradient information and having fewer parameters. Therefore, the whale optimization algorithm (WOA) is employed to optimize the relevant parameters of the maximum correlated kurtosis deconvolution (MCKD) technique. The WOA's ability to explore and exploit the search space efficiently, by mimicking the hunting behaviors of whales, makes it a suitable choice for tuning the parameters of the MCKD method in order to enhance its performance.

The WOA involves three processes: surrounding prey, hunting behavior, and searching for prey, as shown below:

(1) **Surrounding prey**. Using a mathematical model to describe the process of whales surrounding their prey, the expression can be described as

$$D = |CW_{best}(t) - W(t)| \tag{20}$$

$$W(t+1) = W_{best}(t) - FD \tag{21}$$

where $\boldsymbol{C}$ and $\boldsymbol{F}$ are coefficient vectors; $\boldsymbol{W}(t)$ is the current whale position vector; and t is the current iteration count.

The coefficient vectors $\boldsymbol{C}$ and $\boldsymbol{F}$ can be calculated by the following formulas:

$$\begin{cases} F = 2ac_1 - a \\ C = 2c_2 \\ a = 2 - 2t/T_{max} \end{cases} \tag{22}$$

where $\boldsymbol{c}_1$ and $\boldsymbol{c}_2$ are random vectors distributed in the [0,1] interval; $T_{\max}$ is the maximum number of iterations; a linearly decreases from 2 to 0.

(2) **Hunting behavior**. The behavior of humpback whales swimming towards their prey is a spiral motion, which can be described mathematically as

$$\begin{cases} W(t+1) = W_{best}(t) + D_p e^{bl} cos(2\pi l) \\ D_p = |W_{best}(t) - W(t)| \end{cases} \tag{23}$$

where D_p is the distance between the humpback whale and its prey; b is the constant associated with the spiral motion trajectory; l is a random number in the [−1,1] interval.

In addition, while spiraling towards prey, humpback whales also contract their encirclement. Assuming that the probability of contracting the enclosure is P_i and the probability of choosing a spiral to update the position of the humpback whale is $1 - P_i$, then there is

$$W(t+1) = \begin{cases} W_{best}(t) - FD, p < P_i \\ W_{best}(t) + D_p e^{bl} cos(2\pi l), p \geq P_i \end{cases} \tag{24}$$

If the value of a decreases when approaching prey, the fluctuation range of vector $\boldsymbol{F}$ also decreases accordingly. During the iteration process, the value of a decreases from 2 to 0, and $\boldsymbol{F}$ is a random value of $[-a, a]$. The next position of a humpback whale lies somewhere between its current location and that of its prey, and the smaller the $\boldsymbol{F}$, the smaller the walking step.

(3) **Searching for prey**. Using a mathematical model to describe the process of a humpback whale searching for prey, the expression can be described as

$$D = |CW_{rand}(t) - W(t)| \tag{25}$$

$$W(t+1) = W_{rand}(t) - FD \tag{26}$$

where $W_{rand}(t)$ is the randomly selected location of the humpback whale.

If $\boldsymbol{F} \geq 1$, a search agent is randomly selected, and the position of other humpback whales will be updated according to the position of the randomly selected, enhancing the overall search capability of the WOA. The specific implementation process of the WOA is shown in **Figure 3**.

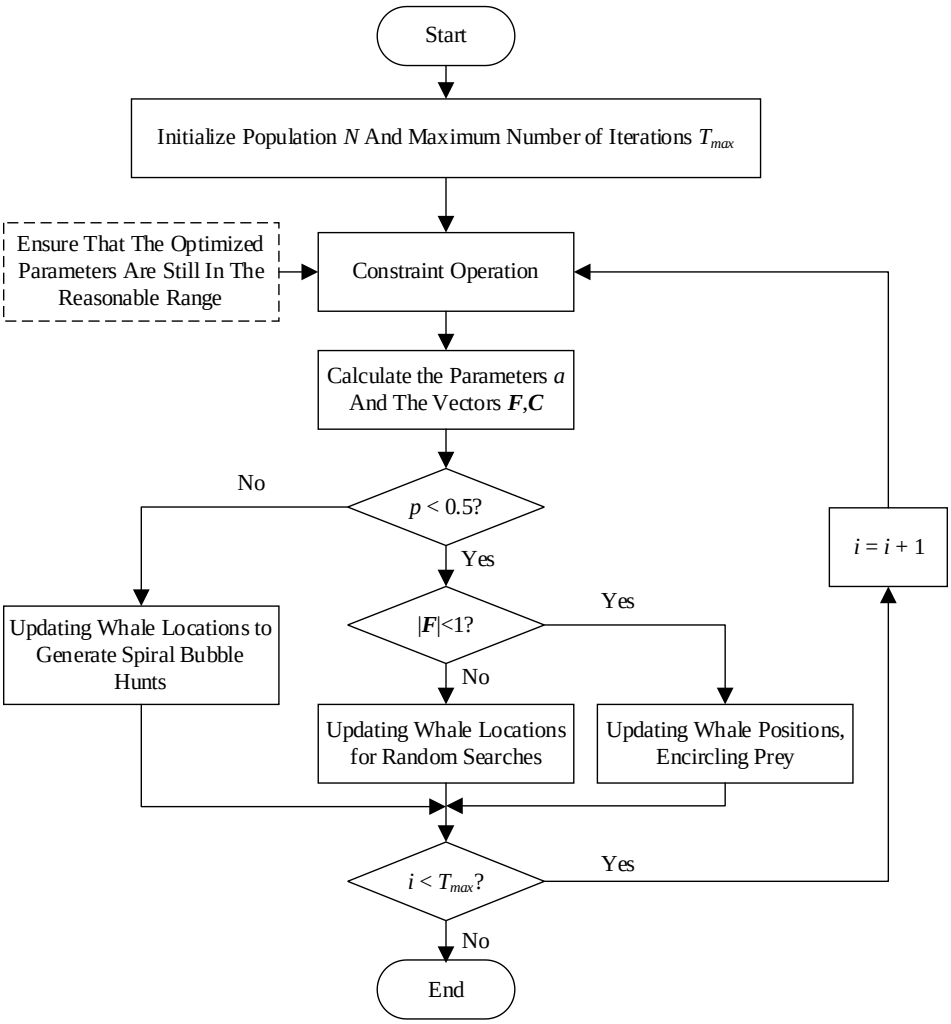

Figure 3. Flowchart of the WOA algorithm.

The WOA algorithm comprises six fundamental steps:

Step 1: Initialize settings. The initial position of the humpback whale is $\boldsymbol{W}_0$, the population of humpback whales is N, and the maximum number of iterations is $T_{\max}$.

Step 2: Evaluate the fitness of each humpback whale, determine whether the parameters are within the constraint interval, find the humpback whale currently in the optimal position within the constraint interval, and save it.

Step 3: Calculate the parameters and coefficient vectors, and determine if the probability P_i is less than 0.5. If so, proceed to step 4; otherwise, update the position of the humpback whale according to Equations (20)–(21).

Step 4: If the absolute value of the coefficient vector F is less than 1, the humpback whales will surround the prey and update their positions accordingly according to Equations (20)–(21). Otherwise, search for prey globally randomly and adjust the position of the humpback whale according to Equations (25)–(26).

Step 5: When the position update is complete, reevaluate the fitness of each humpback whale and compare it to the best-performing whale from the previous iteration. If it is optimal, replace it with the latest optimal solution.

Step 6: Finally, check if the maximum number of iterations has been reached; if it has been reached, the optimal solution is obtained; otherwise, continue to iterate.

By optimizing MCKD through the WOA, the optimal parameter values for filter step size and period can be quickly obtained, improving the accuracy of the algorithm.

3. Bearing fault diagnosis based on SGMD and WOA-MCKD

Firstly, SGMD decomposes raw signals into noise-reduced SGCs, mitigating mode mixing and preserving non-periodic features. Then, MCKD enhances fault-related impulses within SGMD's SGCs, leveraging its cyclization amplification. Lastly, WOA optimizes MCKD parameters dynamically, adapting to varying noise levels and fault characteristics. The SGMD and WOA-MCKD methods are used for feature extraction and diagnosis of weak bearing faults under strong noise background. The specific diagnosis process is as follows.

(1) **Data acquisition**. The original vibration signals $\boldsymbol{x}(t)$ of the normal and outer elements of the rolling bearing can be obtained through sensors.

(2) **Signal decomposition based on SGMD**. The SGMD method is used to perform multimodal decomposition on the collected original vibration signals $\boldsymbol{x}(t)$; multiple symplectic geometric components (SGC) are obtained, and the correlation criterion is used to select the SGC with high correlation and reconstruct the signal.

(3) **MCKD optimization based on WOA**. The WOA is used to optimize the parameters of MCKD and obtain the optimal filter step size and period, and the study factor $c_1 = c_2 = 2$.

(4) **Feature extraction**. The obtained optimal filtering step size and period are substituted into MCKD to achieve feature extraction of the reconstructed signal.

(5) **Fault diagnosis**. The envelope spectrum analysis method is used to demodulate the signal envelope and compare the theoretical fault characteristic frequency values of the bearing against the distinct peak spectral lines in the envelope spectrum to diagnose the specific fault type.

According to the above diagnosis process, the bearing fault diagnosis flowchart based on SGMD and WOA-MCKD is shown in **Figure 4**.

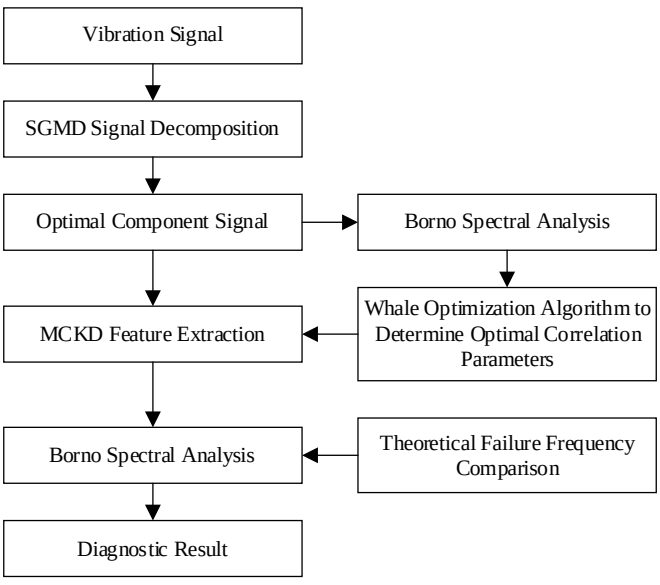

Figure 4. Flowchart of fault diagnosis based on SGMD and WOA-MCKD.

4. Experimental verification and result analysis

4.1. Simulation verification

Firstly, to verify the effectiveness and feasibility of the algorithm proposed in the article, early outer ring faults of rolling bearings are simulated [17]. To simulate the strong noise environment of the rotor, Gaussian functions are used for simulation, and the expression of the simulation signal is as follows:

$$\begin{cases} x(t) = s(t) + n(t) = \sum_i A_i h(t - iT - \tau_i) + n(t) \\ h(t) = exp(-Ct)\, sin(2\pi f_n t) \\ A_i = A_0\, sin(2\pi f_r t) \end{cases} \tag{27}$$

where $x(t)$ is the collected vibration signal; $s(t)$ is the fault signal component; $n(t)$ is the white noise signal; A_0 is the initial vibration amplitude; C is the attenuation coefficient; f_n is the resonance frequency; f_r is the bearing rotation frequency; and τ_i is the small fluctuation of the i-th impulse, which can be set as a random value. Taking the values A_0 = 0.8, f_n = 5000 Hz, f_r = 300 Hz, and C = 1000, the waveform of the impulse signal is shown in **Figure 5**. As shown in the figure, the signal exhibits non-periodic and non-stationary characteristics. By adding Gaussian white noise $n(t)$ with a signal-to-noise ratio of −12 dB, the waveform of the collected vibration signal is shown in **Figure 6**. The FFT transformation is performed on it, and the frequency spectrum of the vibration signal is shown in **Figure 7**. From **Figures 6** and **7**, it can be seen that the original vibration signal is not significantly different from white noise, and the frequency spectrum of the original signal cannot accurately obtain obvious prominent components.

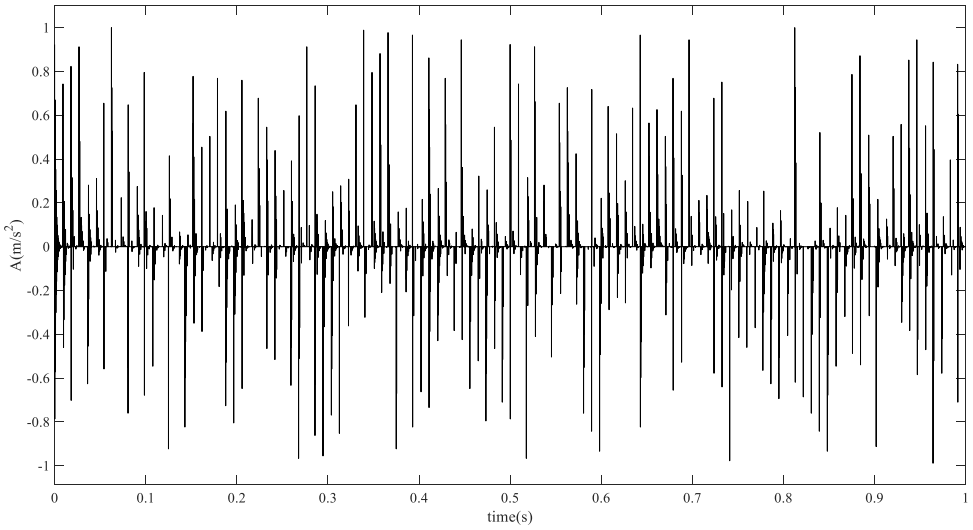

Figure 5. Waveform of the impulse signal.

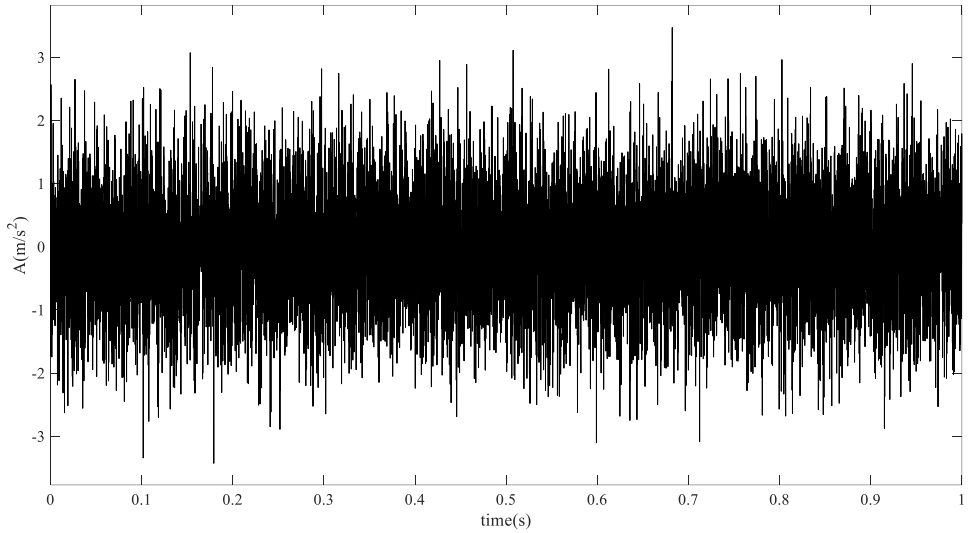

Figure 6. Waveform of the vibration signal with strong noise.

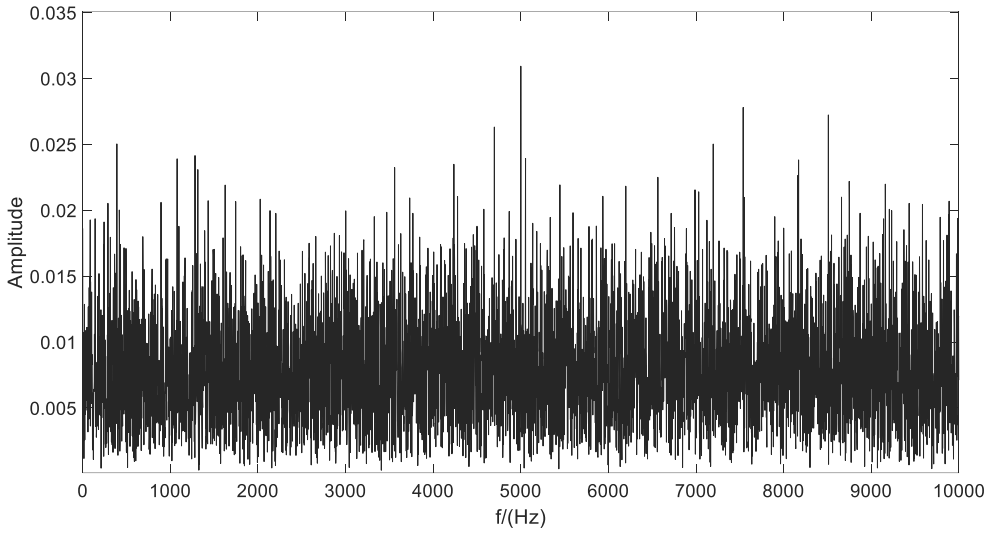

Figure 7. Spectrum diagram of the original signal.

For the non-periodic, non-stationary, and strong noise vibration signals of the rolling bearing in **Figure 7**, VMD and SGMD are selected for decomposition, and their signal envelope spectra are shown in **Figures 8** and **9**, respectively. The comparison results show that VMD and SGMD algorithms can extract frequency components around 110 Hz, but the decomposition effect of SGMD for non-periodic and non-stationary is better than that of VMD.

The filter length parameter L and deconvolution period T of MCKD significantly influence its performance. The energy characteristics of the decomposed signal under these parameters are illustrated in **Figure 10**. The results indicate that further determination of the optimal filter length parameter and deconvolution period is required.

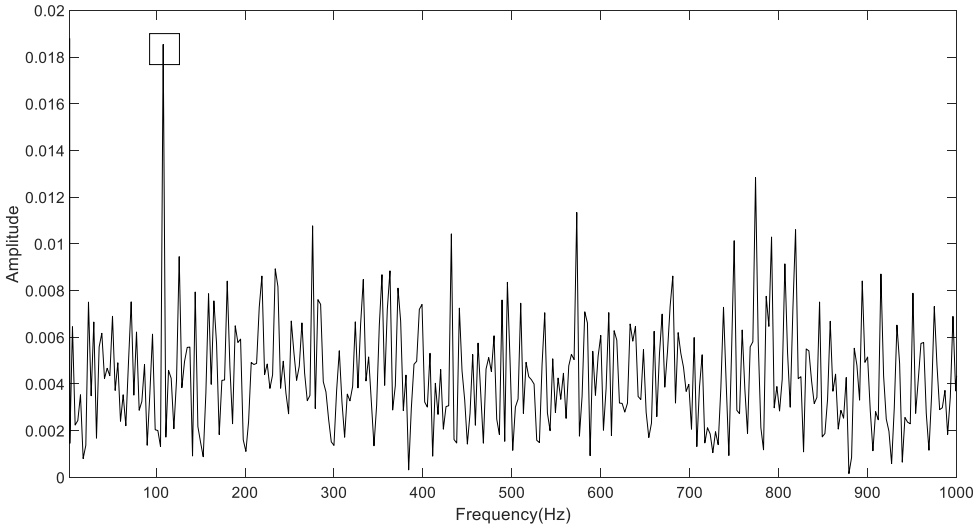

Figure 8. Frequency envelope diagram of signals based on VMD.

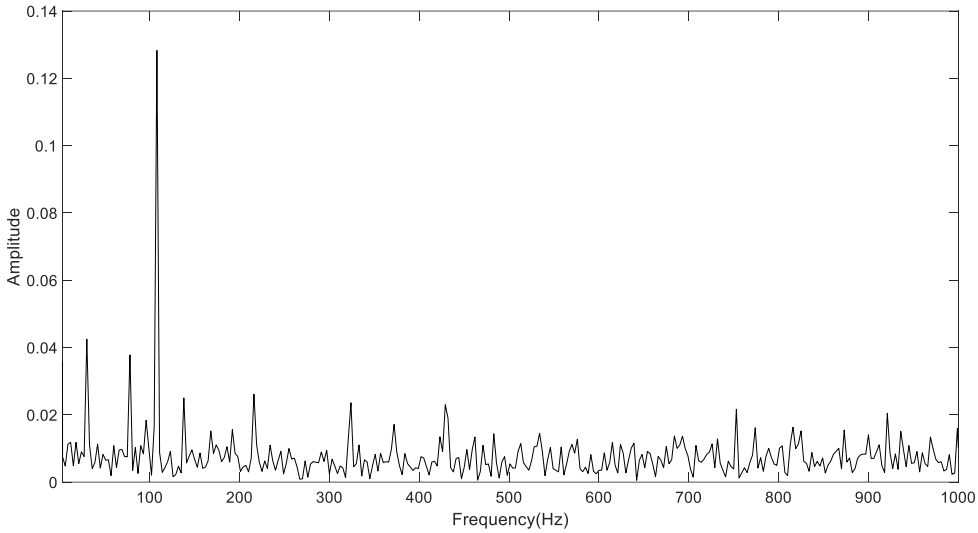

Figure 9. Frequency envelope diagram of signals based on SGMD.

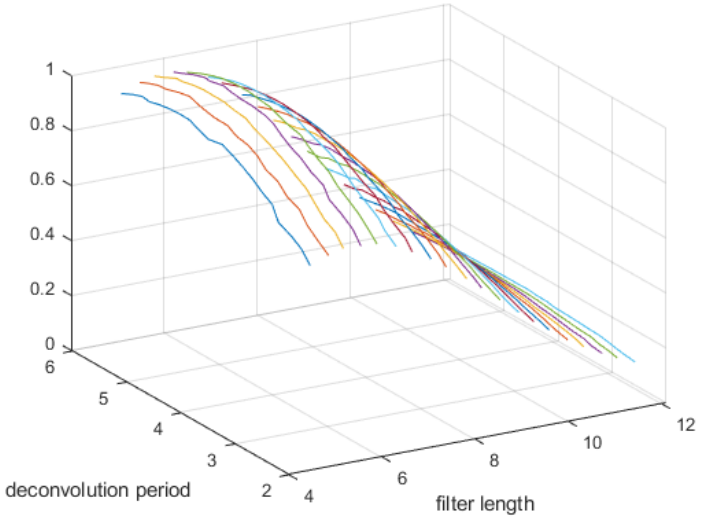

Figure 10. Energy Characteristics of MCKD Under different deconvolution period and filter length parameters.

To achieve the optimal decomposition effect of MCKD, the WOA is used for optimization. The objective function is to maximize the frequency envelope variance. The optimization results of parameters based on WOA-MCKD, PSO-MCKD, and GE-MCKD are shown in **Figure 11**, and their optimal decomposition effect is shown in **Figure 11**. From **Figure 10**, the WOA-MCKD is better than PSO-MCKD and GE-MCKD. Compared with **Figure 9**, it can be seen that the frequency prominent part of the signal is more obvious.

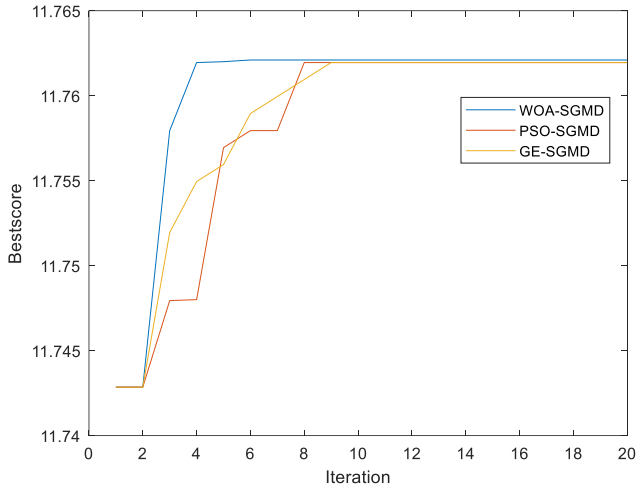

Figure 11. Parameter optimization based on WOA-MCKD, PSO-MCKD, and GE-MCKD.

As shown in **Figure 12**, except for the prominent frequency component around 110 Hz, other frequencies are not effective. To further highlight the regular impulse components, the MCKD is used for feature extraction. To achieve the optimal decomposition effect of the MCKD, the WOA is also used to optimize the parameters of the MCKD. The optimization results are shown in **Figure 12**. From **Figure 12**, except for the prominent frequency component around 110 Hz, other frequency components are also prominent and can be utilized for diagnosing faults in rolling bearings.

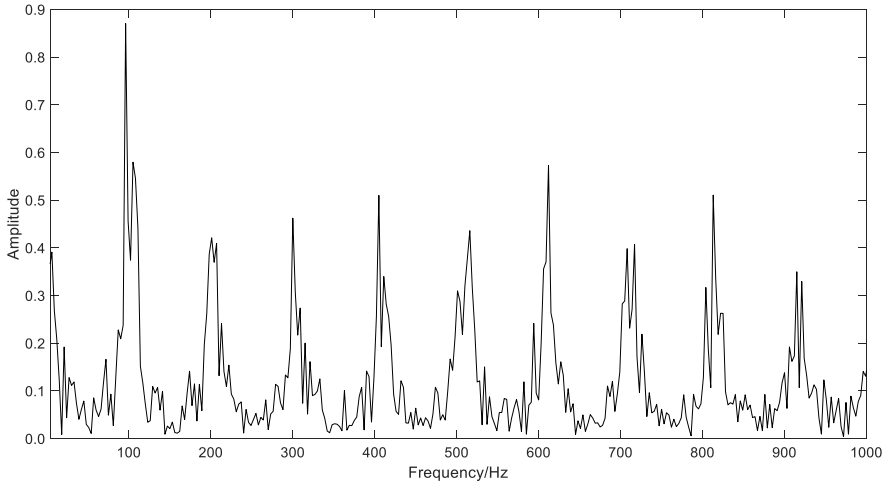

Figure 12. Envelope spectrum of signals based on WOA-MCKD.

Accuracy is defined as the ratio of correctly classified samples (both fault and healthy classes) to the total number of samples in the test dataset, as shown in Equation (28).

$$Accuracy = \frac{TP + TN}{TP + TN + FP + FN} \times 100\% \tag{28}$$

where TP: True positives (correctly identified faulty samples).

TN: True negatives (correctly identified healthy samples).

FP: False positives (healthy samples misclassified as faulty).

FN: False negatives (faulty samples misclassified as healthy).

To demonstrate the superiority of the proposed WOA-SGMD-MCKD algorithm, EMD-GA-BP [18], OEGOA-VMD, SSA-MCKD, VMD-MCKD, LSTM, and the proposed algorithm in the paper are selected for comparison, as shown in **Table 1**. The experimental results show that EMD has the lowest accuracy and the proposed algorithm has the highest accuracy, which can satisfy the practical requirements.

Table 1. Accuracy of different weak fault diagnosis algorithms in roll bearings.

The fault diagnosis algorithm	Accuracy
EMD-GA-BP [19]	65.33%
OEGOA-VMD [20]	78.21%
SSA-MCKD [21]	79.78%
VMD-MCKD [22]	81.79%
LSTM [23]	82.14%
WOA-SGMD-MCKD	85.64%

4.2. Experimental verification

The algorithm proposed in this paper is validated using a motor propeller tension experimental platform, as shown in **Figure 13**. The platform can offer unparalleled flexibility, safety, and efficiency for engineers and developers in the UAV industry and comprehensive tools for real-time data interpretation and one-click test report generation. The system is capable of high-speed sampling at 10 kHz, and manual wear marks are added to the outer ring of the rolling bearing. The origin signals are collected through vibration sensors, and the parameters of the rolling bearing are shown in **Table 2**.

Figure 13. Motor propeller tension experimental platform.

Table 2. Parameters of the rolling bearing.

Bearing type	Outer diameter /mm	Inner diameter /mm	Width/mm
MR85zz	8	5	2.5

The vibration signal waveforms of bearings without faults and bearings with faults are shown in **Figures 14** and **15**. It can be seen that fault signals of bearings are difficult to distinguish directly.

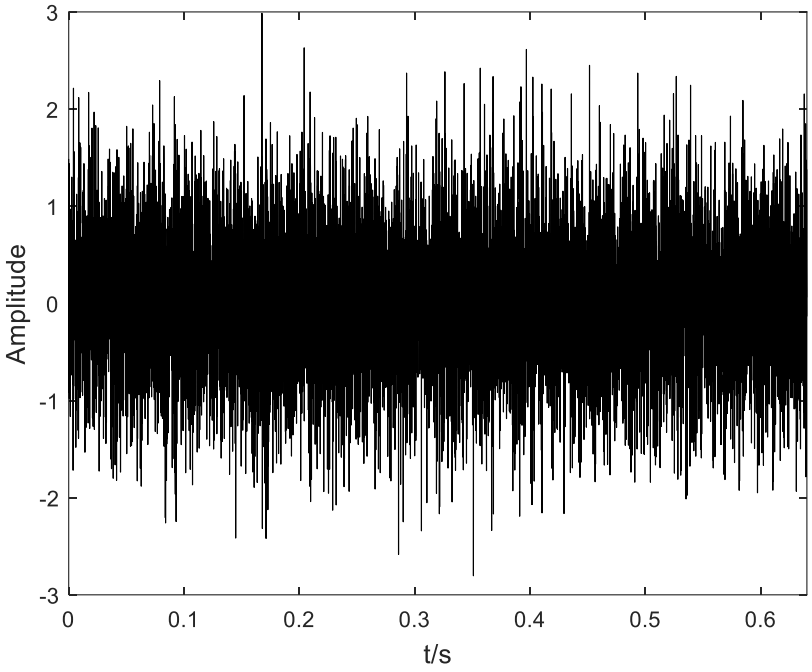

Figure 14. Vibration signals of bearings without faults.

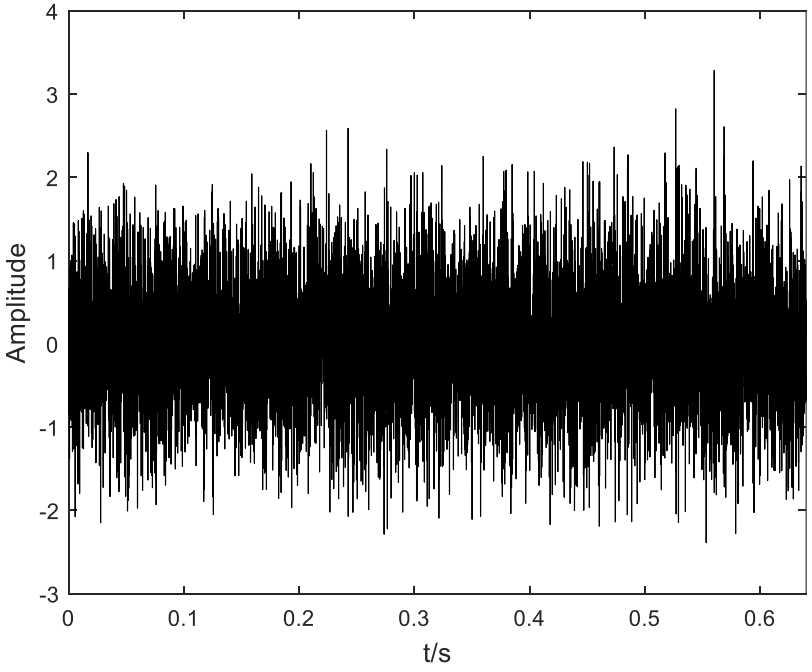

Figure 15. Vibration signals of bearings with weak faults.

The WOA-SGMD-MCKD method proposed in the paper is used to extract the envelope spectrum of vibration signals, and the results are shown in **Figure 16**. From **Figure 15**, the deconvolution signal of the normal state has a significant spectral peak near 110 Hz and insignificant spectral peaks in other frequency domains, whereas the deconvolution signal of the faulty state has a significant spectral peak at the high harmonics. This shows the effectiveness and feasibility of the algorithm proposed in this paper.

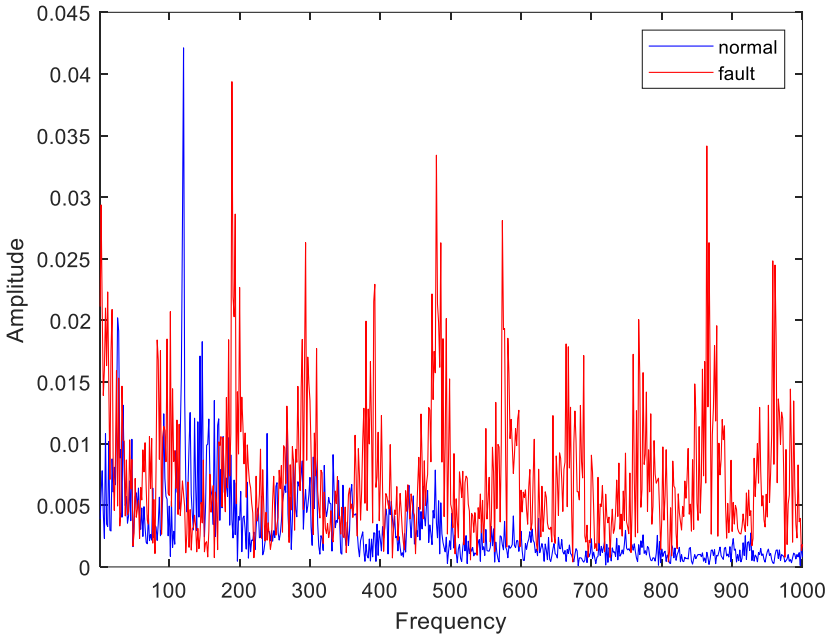

Figure 16. Envelope spectrum of vibration signals based on WOA-SGMD-MCKD.

5. Conclusions

The rolling bearings of rotor blades are prone to structural damage in harsh environments such as strong vibration and salt spray. Aiming at the characteristics of non-periodic, non-stationary, and strong noise of bearing fault signals in rotor blades, this paper introduces a novel early fault diagnosis algorithm leveraging the integration of WOA, SGMD, and MCKD. Firstly, the original fault signal is processed by SGMD to get its impulse component; in order to get the optimal decomposition effect of the SGMD, the WOA is adopted to optimize the SGMD in this paper, and at the same time, in order to enhance the extraction effect of the impulse signal of the MCKD, the WOA is also used for parameter optimization. Both simulation and experimental outcomes demonstrate the efficacy of the proposed algorithm in accurately diagnosing non-periodic and non-stationary early fault signals emanating from rotor bearings. However, it is necessary to preset the fault frequency range in advance. If the actual fault frequency exceeds the preset range (e.g., high-frequency resonance), it may lead to failure in extracting fault features.

Author contributions: Conceptualization, LG and CHL; methodology, CHL; software, LG; validation, LG and CHL; formal analysis, LG; investigation, LG; resources, CHL; data curation, CHL; writing—original draft preparation, LG;

writing—review and editing, LG and CHL; visualization, LG and CHL; supervision, CHL; project administration, CHL; funding acquisition, CHL. All authors have read and agreed to the published version of the manuscript.

Institutional review board statement: Not applicable.

Informed consent statement: Not applicable.

Conflict of interest: The authors declare no conflict of interest.

References

1. Kumar N, Satapathy RK. Bearings in aerospace, application, distress, and life: A review. Journal of Failure Analysis and Prevention. 2023; 23(3): 915–947.
2. Skowron M, Frankiewicz O, Jarosz JJ, et al. Detection and Classification of Rolling Bearing Defects Using Direct Signal Processing with Deep Convolutional Neural Network. Electronics. 2024; 13(9): 1722.
3. Peng B, Bi Y, Xue B, et al. A survey on fault diagnosis of rolling bearings. Algorithms. 2022; 15(10): 347.
4. Li J, Luo W, Bai M. Review of research on signal decomposition and fault diagnosis of rolling bearing based on vibration signal. Measurement Science and Technology. 2024; 35(9).
5. Hou Y, Wang J, Chen Z, et al. Diagnosisformer: An efficient rolling bearing fault diagnosis method based on improved Transformer. Engineering Applications of Artificial Intelligence. 2023; 124: 106507.
6. Cao D, Gu Y, Lin W. Fault Diagnosis Based on Optimized Wavelet Packet Transform and Time Domain Convolution Network. Transactions of FAMENA. 2023; 47(3): 1–14.
7. Chen T, Guo L, Gao H, et al. Clustering Weighted Envelope Spectrum for Rolling Bearing Fault Diagnosis. IEEE Transactions on Automation Science and Engineering. 2024; 22: 3922–3932.
8. Pu H, Zhang K, An Y. Restricted sparse networks for rolling bearing fault diagnosis. IEEE Transactions on Industrial Informatics. 2023; 19(11): 11139–11149.
9. Meng D, Wang H, Yang S, et al. Fault analysis of wind power rolling bearing based on EMD feature extraction. CMES—Computer Modeling in Engineering & Sciences. 2022; 130(1): 543–558.
10. Gao S, Zhao N, Chen X, et al. A new approach to adaptive VMD based on SSA for rolling bearing fault feature extraction. Measurement Science and Technology. 2023; 35(3).
11. Zhang G, Wang Y, Li X, et al. Enhanced symplectic geometry mode decomposition and its application to rotating machinery fault diagnosis under variable speed conditions. Mechanical Systems and Signal Processing. 2022; 170: 108841.
12. Prawin J. Rolling element bearing fault identification using vibration data. International Journal of Structural Stability and Dynamics. 2023; 25(2).
13. Chen X, Shu G, Zhang K, et al. A fault characteristics extraction method for rolling bearing with variable rotational speed using adaptive time-varying comb filtering and order tracking. Journal of Mechanical Science and Technology. 2022; 36(3): 1171–1182.
14. Miao Y, Li C, Shi H, Han T. Deep network-based maximum correlated kurtosis deconvolution: A novel deep deconvolution for bearing fault diagnosis. Mechanical Systems and Signal Processing. 2023; 189: 110110.
15. LV Y, Wang J, Zhang C, Ding J. Composite fault feature extraction for gears based on MCKD-EWT adaptive wavelet threshold noise reduction. Measurement and Control. 2024; 58(2).
16. Guo Z, Fei H, Liu B, Cao Y. Sparse Representation Based on MCKD and Periodic Dictionary for Bearing Fault Diagnosis. IEEE Transactions on Instrumentation and Measurement. 2024; 73: 1–10.
17. Wang H, Zheng J, Xiang J. Online bearing fault diagnosis using numerical simulation models and machine learning classifications. Reliability Engineering & System Safety. 2023; 234: 109142.
18. Liu Y, Kang J, Bai Y, Guo C. Research on the health status evaluation method of rolling bearing based on EMD-GA-BP. Quality and Reliability Engineering International. 2023; 39(5): 2069–2080.
19. Yang Y, Liu H, Han L, Gao P. A feature extraction method using VMD and improved envelope spectrum entropy for rolling bearing fault diagnosis. IEEE Sensors Journal. 2023; 23(4): 3848–3858.
20. Wang B, Guo Y, Zhang Z, et al. Developing and applying OEGOA-VMD algorithm for feature extraction for early fault detection in cryogenic rolling bearing. Measurement. 2023; 216: 112908.

21. Du Y, Li G. Application of adaptive MCKD method optimized by SSA based on mixed strategy in rolling bearing fault diagnosis. Journal of Advanced Mechanical Design, Systems, and Manufacturing. 2023; 17(5).
22. Ke Z, Liu H, Shi J, Shi B. Fault diagnosis method of weak vibration signal based on improved VMD and MCKD. Measurement Science and Technology. 2024; 35(2).
23. Afridi Y S, Hasan L, Ullah R, et al. LSTM-Based Condition Monitoring and Fault Prognostics of Rolling Element Bearings Using Raw Vibrational Data. Machines. 2023; 11(5): 531.